Solar hybrid road: from numerical model to an energy balance in France

Nicolas Le Touz, Jean Dumoulin, J.M. Piau

SOLAR HYBRID ROAD: FROM NUMERICAL MODEL TO AN ENERGY BALANCE IN FRANCE

N. Le Touz[1,3], J. Dumoulin[1,3], J.-M. Piau[1,2]
[1] IFSTTAR, COSYS-SII, Route de Bouaye-CS4, F-44344, Bouguenais, France
[2] IFSTTAR, MAST, LAMES, F-44344, Bouguenais, France
[3] Inria, I4S Team, Campus de Beaulieu, F-35042, Rennes, France
*Correspondence author: Fax: +33 (0)2 4084 5998
Email: {nicolas.le-touz, jean.dumoulin, jean-michel.piau}@ifsttar.fr

ABSTRACT

In this study, we evaluate the energy to bring to a solar hybrid road system to prevent it from icing at the surface. To estimate the thermal performances, a multiphysics finite element model is introduced to compute the temperature field from environmental conditions. From this model, the adjoint state method is used to solve an optimization problem taking into account a penalization of frozen periods and the energy brought to the system. Results obtained for different climatic conditions in France are presented, analyzed and discussed.

NOMENCLATURE

h_{conv}	convective heat transfer coefficient
h_{rad}	radiative heat transfer coefficient
T	temperature of the solid phase
T_{eq}	equivalent temperature
T_f	temperature of the fluid phase
$T_{\mathrm{f,in}}$	input fluid temperature
T_{ref}	reference temperature
T_{surf}	surface temperature
T_{th}	temperature threshold
h_{fs}	heat transfer coefficient between solid and fluid phases

INTRODUCTION

Energy transition implies the search for new energy sources and energy management. In this context, numerous studies have been led on recovering part of solar radiation. On the other way, car traffic increase entails road network expansion (*i.e.* its surface). These road structures are submitted to environmental conditions (*i.e.* thermal variations). Thus, during summer, high temperature and solar radiation conditions provoke an increasing of temperature in the structure that can entail rutting and contribute to the rise of the heat island effect [8, 14].

However, energy harvesting through adapted pavement structures, can be realized with dedicated heat transfer systems. These solutions can be based on photovoltaic collectors inserted in the road structure and/or heat fluid flowing in buried pipes [5].

On the other hand, winter conditions can provoke black ice occur at the surface of the roads, which is a problem for safety, for environmental preservation when salting [7], and for economy because of traffic flow disruption. Solutions for preventing surface from icing are actually mainly based on electrical or geothermal heating techniques [4].

We propose here to control the temperature of the road structures with a modified system acting as a thermal exchanger, able to bring energy during winter and to recover energy during summer. Traditional approaches aiming at building such embedded energetic system rely on tubes buried below the surface layer of the pavement [8]. In this study, we present a solar hybrid road in which a heat fluid flows inside a porous layer inserted below the surface layer. A first study of such porous solution was presented in [1] but only for established permanent regime. In the present study, in addition to this porous layer, a semi-transparent surface layer is added to the structure surface to favour solar radiation penetration (toward greenhouse effect) and calculation are conducted in dynamic regime.

This concept of hybrid solar road is detailed in the first part of this study. Then, finite element method to compute the temperature field in the structure is presented. This method allows to introduce a control law relying on adjoint state method to prevent the surface from icing. Needs of energy to achieve this objective are finally presented and discussed for some locations.

HYBRID SOLAR ROAD CONCEPT

Hybrid solar road is a multilayer system for which the two layers closest to the surface are modified compared to traditional road structures. A schematic view of hybrid solar road and interactions with environment are shown in figures 1 and 2.

λ	$[0, 0.5]$	$[0.5, 2.7]$	$[2.7, 4.5]$	$[4.5, 50]$	≥ 50
κ	0	10	1000	5000	$+\infty$
σ_s	10	10	10	10	10

MULTI-PHYSIC NUMERICAL MODEL

We present in this part our numerical model combining thermal diffusion, hydraulic convection and radiative heat transfer with the finite element method. Applying this method allows in particular to keep the same spatial mesh for these three problems without interpolation.

Thermal diffusion

The structure is subject to thermal diffusion. Interactions with the environment come from convection with the air, radiation with the sky and solar radiation. The depth of the structure is supposed to be large enough so that thermal exchanges at boundaries can be neglected except at the surface S (see figure 2) where Robin boundary conditions are considered.

$$\begin{cases} \rho C_p \dfrac{\partial T}{\partial t} = \nabla \cdot [k\nabla T] + q \\ k\nabla T \cdot \vec{n} = \begin{cases} \Phi_s + h_c(T_{\text{air}} - T) \\ + h_r(T_{\text{sky}} - T) & \text{on } S \\ 0 & \text{elsewhere} \end{cases} \end{cases} \tag{1}$$

Hydraulic convection

Porous layer is supposed to be saturated in fluid. Flow is governed by Darcy law. Two temperature fields are used: T for the solid phase which is the continuation of the temperature field for non-porous layers and T_f for the fluid phase.

Navier-stokes equations can be integrated over a representative elementary volume to get a coupled system between T and T_f, with the hypothesis of stationary flow as long as weak and uniform porous velocity [2, 15] :

$$(1 - \varphi)\rho C_p \frac{\partial T}{\partial t}$$
$$= (1 - \varphi)\nabla \cdot [k\nabla T] + h_{fs}(T_f - T) \tag{2}$$
$$\varphi \rho_f C_{p,f} \frac{\partial T_f}{\partial t} + \rho_f C_{p,f} u \cdot \nabla T_f$$
$$= \varphi \nabla \cdot [k_f \nabla T_f] + h_{fs}(T - T_f) \tag{3}$$

With h_{fs} an exchange coefficient between fluid and solid phase. This coefficient can be obtained from pore characteristics [15].

Equation (3) is hyperbolic because of the advection term. Solving this system with the Galerkin method
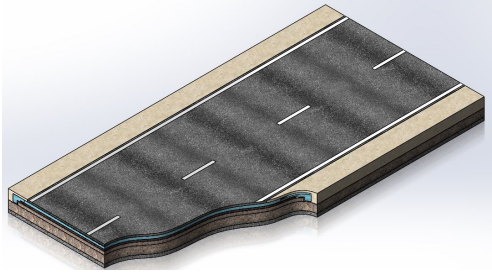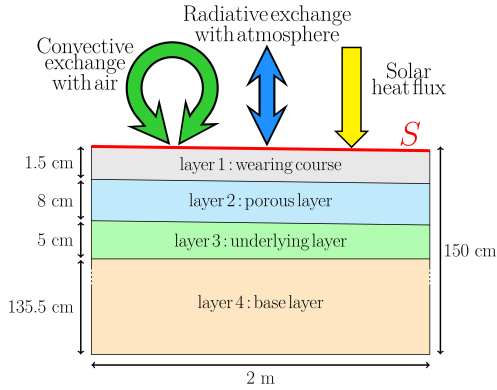

Figure 1: Schematic view of solar hybrid road

Figure 2: Solar hybrid road structure and interactions with the environment

Layer 1 is a semi-transparent medium: solar radiation can penetrate deeply in the structure and even more impact porous layer 2 in which a fluid flows through the width of the road, thanks to the effect of the imposed slope. Other layers 3 and 4 are similar to traditional roads and are also opaque and waterproof. Thermal properties of considered materials are reported in table 1.

Table 1
Thermal properties of sublayers for numerical simulations [1, 10, 17]

	layer 1	layer 2	layer 3	layer 4	fluid
k	0.85	1.03	1.40	1.10	0.60
ρ	2700	2360	2620	2300	1000
C_p	840	780	860	1000	4180

In a first approach, optical properties are taken as given by [16] and estimated with an experimental mock-up [13]. These properties are reported in table 2. Optical properties are a function of wavelength. The semi-transparent layer is designed to be transparent to solar radiation wavelengths and opaque for ambient radiation wavelengths.

Table 2
Optical properties of the semi-transparent layer as a function of wavelength λ (in μm)

can also entail spurious oscillation on the numerical solution. To avoid this problem, we use the Petrov-Galerkin formulation. Interpolation functions are modified to add numerical diffusion [11].

Radiative heat transfer in the semi-transparent surface layer

Radiative transfer occurring in the semi-transparent layer are governed by the radiative transfer equation (4). Solving this equation allows to get the intensity (directional radiative flux) in the semi-transparent layer.

$$\omega \nabla I_\nu = -(\kappa + \sigma_s)I_\nu + \kappa B_\nu(T) + \frac{\sigma_s}{4\pi}\int_{4\pi}\Phi I_\nu d\omega \tag{4}$$

With $B_\nu(T)$ the blackbody emission for frequency ν at temperature T.

The transition term is neglected here. In fact, dimensions of the domain are such that radiative equilibrium is reached quite instantaneously.
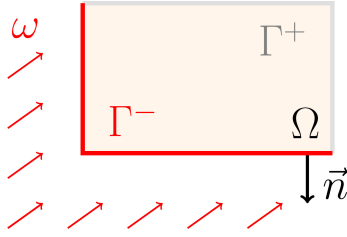

Figure 3: Input boundaries for radiative transfer

The intensity on the input boundary Γ^- shown in figure 3 comes from internal reflection g_{in} and external contribution g_{out}. Intensity in Γ^- is written:

$$I_\nu(s,\omega) = g_{in}(s,\omega,I_\nu) + g_{out}(s,\omega) \tag{5}$$

To solve the radiative transfer equation and to get the intensity field, two discretizations are required: in direction and space. For directional discretization, the method of discrete ordinates is applied. For each direction of the angular mesh, RTE equation (4) is written for this direction and integral terms become sums on angular mesh. A semi-discrete system is also obtained. In this study, we use an icosahedron as a directional mesh, which allows to get a regular mesh and also not to favor some directions. This icosahedron can be refined recursively to improve mesh refinement [12].

Variation of radiative energy $\omega \cdot \nabla I_\nu$ can be assimilated to an advection term. A stabilization technique is also required to apply the finite element method. As for equation (3), We use the Petrov-Galerkin method on each semi-discrete equation. A linear discretized system is also obtained.

The energy that is absorbed in the semi-transparent medium or at interfaces with opaque layers can be computed from the intensity field [9].

Numerical coupling

A scheme of the numerical coupling for each time step is shown in figure 4. First, knowing the current temperature field and environmental conditions, radiative transfer equation is solved to get the intensity field, which allows to compute heat sources. These sources are injected in thermal diffusion equation, which is solved with hydraulic convection equation and a Crank-Nicolson scheme. The temperature field at the next time step is thus obtained.
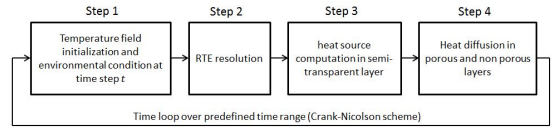

Figure 4: Temporal scheme

COMMAND LAW FOR THE INPUT TEMPERATURE OF THE FLUID

We present in this paragraph the approach developed to control the surface temperature of the structure under adverse weather conditions during winter.

The aim is to find the input fluid temperature $T_{\text{f,in}}$ such as the surface temperature T_{surf} is higher than a given set-point T_{th} and the energy needed to heat the fluid is minimal. The set-point needs to be such that there is no risk of icing.

We introduce a functional J composed of two terms: a residual term to take into account the difference between the threshold and the surface temperature when the first is higher than the second and a Tikhonov term, which allows to take into account the energy needed to heat the input fluid from a reference temperature $T_{\text{f,ref}}$ to $T_{\text{f,in}}$ at the same time:

$$J = \frac{1}{2}\int_S\int_t ((T_{\min}-T)^+)^2 dSdt + \frac{\epsilon}{2}\int_t (T_{\text{f,in}}-T_{\text{f,ref}})^2 dt \tag{6}$$

Where $(\cdot)^+$ is the positive part. We note $\mathscr{M} = L^2(S,[0,t_a])$ the measure space with t_a the time horizon, $\|\cdot\|_{\mathscr{M}}$.

With these notations, the functional J becomes:

$$J = \frac{1}{2}\|(T_{\min}-T)^+\|^2_{\mathscr{M}} + \frac{\epsilon}{2}\|T_{\text{f,in}}-T_{\text{f,ref}}\|^2_{\mathscr{U}} \tag{7}$$

We use the conjugate gradient method to minimize J, which requires to calculate the gradient of the functional. The unknown $T_{\text{f,in}}$ is explicit in the Tikhonov term. For the residual term, the unknown appears in

T via the model. We use the adjoint state method to compute the gradient of the residual term.

From the direct model presented above, the effects of infinitesimal variations $\delta T_{\text{f,in}}$ of the input fluid temperature on the surface temperature field can be computed with the linear tangent model. Given that the direct model is linear in $T_{\text{f,in}}$, both direct and linear tangent model are equivalent. The adjoint problem (8) can be deduced.

$$
\begin{cases}
\begin{cases}
-(1-\phi)\rho c_p \dfrac{\partial \delta T^*}{\partial t} - (1-\phi)\nabla \cdot (k \nabla \delta T^*) \\
= (T_{\min} - T)^+ \delta_S + \begin{cases} h(\delta T_f^* - \delta T^*) \text{ on } \Omega_f \\ 0 \text{ on } \Omega \setminus \Omega_f \end{cases} \\
\delta T^*(t = t_a) = 0 \\
k \nabla \delta T^* \cdot \vec{n} = -(h_{\text{conv}} + h_{\text{rad}})\delta T^* \text{ on } S \\
k \nabla \delta T^* \cdot \vec{n} = 0 \text{ on } \partial\Omega \setminus S
\end{cases} \\
\begin{cases}
-\phi(\rho c_p)_f \dfrac{\partial T_f^*}{\partial t} - (\rho c_p)_f \vec{u} \cdot \nabla \delta T_f^* \\
-\nabla \cdot (k_f \nabla \delta T_f^*) = h(\delta T^* - \delta T_f^*) \\
\delta T_f^*(t = t_a) = 0 \\
\delta T_f^* = 0 \text{ on } \Gamma_{\text{f,in}} \\
k_f \nabla \delta T_f^* \cdot \vec{n} = -(\rho c_p)_f \delta T_f^* \vec{u} \cdot \vec{n} \text{ on } \partial\Omega_f \setminus \Gamma_{\text{f,in}}
\end{cases}
\end{cases}
\tag{8}
$$

Where δ_S is the Heaviside function for the surface. Adjoint and direct problem have the same structure. The same method, presented before, can be applied to solve both problems.

The gradient of the functional is expressed as:

$$
\begin{aligned}
J'(\delta T_{\text{f,in}})\delta \tilde{T}_{\text{f,in}} \\
= -\int_{t=0}^{t_a} \int_{\Gamma_{\text{f,in}}} \delta \tilde{T}_{\text{f,in}} \left(k_f \nabla \delta T_f^* \cdot \vec{n} \right. \\
\left. + (\rho C_p)_f \delta T_f^* \vec{u} \cdot \vec{n} \right) \mathrm{d}S\mathrm{d}t \\
+ \epsilon \int_{t=0}^{t_a} \delta \tilde{T}_{\text{f,in}}(T_{\text{f,in}} - T_{\text{f,ref}})\mathrm{d}t
\end{aligned}
\tag{9}
$$

Solution of direct and adjoint problems allow also to compute the gradient of the functional and to perform the conjugate gradient method.

APPLICATION TO ICE PENVENTING

Considerations on surface temperature threshold

In a first approach, the surface temperature set-point is considered as constant and positive. To ensure a safety margin, we can impose $T_{\text{th}} = +4°C$.

However, black ice occurs if water vapor solidifies while air temperature decreases to the frozen point T_{f}. For a dry air, the frozen point can be much lower than $0°C$ and there is also no risk of black ice beyond T_{f}, particularly for negative temperature.

Frozen point can be computed from water vapor pressure in the air p_w [3].

$$
T_{\text{f}} = \frac{c_g \ln(p_w/a_g)}{b_g - \ln(p_w/a_g)}
\tag{10}
$$

With $a_g = 6.1115$, $b_g = 22.452$ and $c_g = 272.55$ K. Finally, two surface temperature set-points are considered: first one is constant, such as $T_{\text{th}} = 4°C$. The second is linked to the frozen point: $T_{\text{th}} = \min(4°C, T_{\text{f}} + 4)$.

Weather data are extracted from RT 2012 and Energy Plus [6] and are supposed to match with weather predictions. Input fluid temperature is computed as follows from these data: for each day (time t_0), the initial thermal state of the system is supposed to be known and weather data prediction for the next 4 days are supposed to be available. Direct model is applied, with a constant input fluid temperature ($T_{\text{f,in}} = 13°C$) to compute the surface temperature. The optimization problem is solved to obtain the optimal input fluid temperature. The new thermal state prediction is also computed at pre-defined time step. The procedure is repeated with weather predictions updates. We applied this procedure to a full year weather data set for different locations.

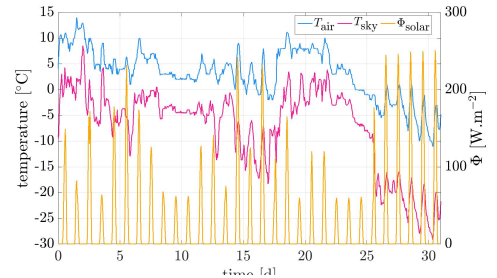Examples of weather conditions on one month for Nancy and Rennes are shown in figures 5 and 6.

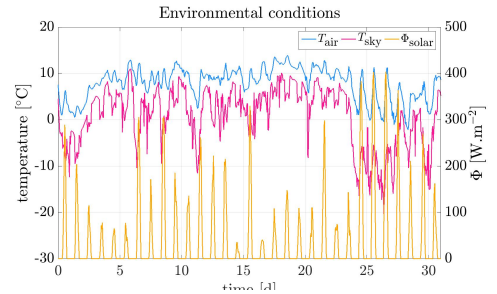Figure 5: Environmental conditions in Nancy

Figure 6: Environmental conditions in Rennes

Applying the direct model allows to get the minimal surface temperature at each time step. The surface temperature set-points (Static and Dynamic) are also shown in figures 7 and 8.
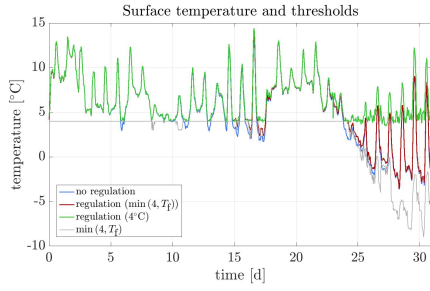
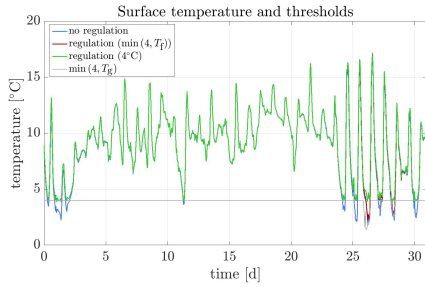Figure 7: Evolution of minimal temperature at the surface in Nancy

Figure 8: Evolution of minimal temperature at the surface in Nancy

The computed input fluid temperatures for both surface temperature set-points are shown in figures 9 and 10.
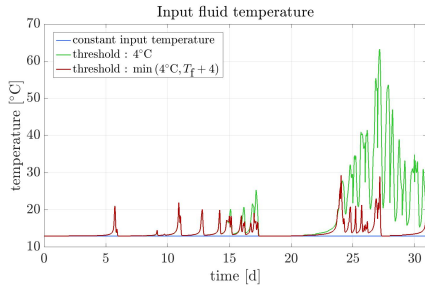

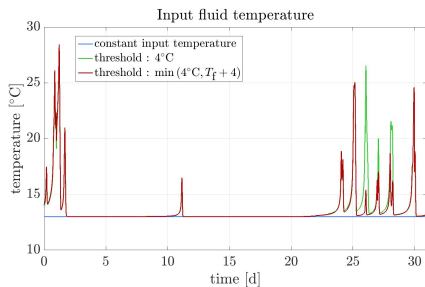Figure 9: Input fluid temperature in Nancy

Figure 10: Input fluid temperature in Rennes

For both surface temperature set-points, the surface temperature is higher than the threshold. During adverse environmental conditions, the minimal surface

temperature tangents the threshold. Because the constant threshold is higher than the dynamic threshold, based on frozen point, the input fluid temperature is higher in the first case, entailing higher energy consumption to heat the fluid. The maximum input fluid temperature is, as shown in figure 9, about 65°C in the first case against about 30°C in the second case. Less effects (potential energetic gains) are observed for Rennes location due to wet winter climate. In addition to energy saving, this decrease of input fluid temperature allows to prevent material degradations in the porous layer of the road due to a too high inlet temperature.

Estimation of energy consumption:
In this section, we evaluate energy required to prevent the surface from icing. The energy per unit surface E to heat the input fluid is computed by integrating the difference between the reference $T_{f,ref}$ and the computed input temperature $T_{f,in}$:

$$E = \frac{1}{S} \int_t \dot{m} \rho c_p (T_{f,in} - T_{f,ref}) \mathrm{d}t \qquad (11)$$

Where S is the surface to prevent from icing.

Such evaluation procedure is applied to four locations subjected to various climates: Aix-en-Provence, Madrid, Nancy and Rennes. Aix-en-Provence is submitted to a mediterranean climate, with warm winter. Madrid and Nancy are submitted respectively to degraded mediterranean and oceanic climates with a continental influence which implies cold and dry winters. Rennes is under an oceanic climate with warm and wet winters.

Results obtained for Aix-en-Provence, Madrid, Nancy and Rennes, are presented hereafter (Table 3).

Table 3: Energy balance for Aix-en-Provence, Madrid, Nancy and Rennes

location	$E(T_{min,1})$	$E(T_{min,2})$	δ [%]
Aix-en-Provence	78.15	28.19	63.9
Madrid	70.43	8.13	88.5
Nancy	198.55	54.99	72.3
Rennes	56.12	43.50	22.5

In this table, $E(T_{th,1})$ and $E(T_{th,2})$ refers to the energy per unit surface necessary to heat the fluid for respectively the thresholds $T_{min,1} = 4°C$ and $T_{min,2} = \min(4°C, T_f + 4)$. δ refers to the difference between $E(T_{th,1})$ and $E(T_{th,2})$.
Humidity can be important for surface temperature set-point and energy consumption for some climatic

conditions. For the oceanic climate in Rennes, frozen point is often close to the air temperature around $0°C$, what entails a few difference between $E(T_{\min,1})$ and $E(T_{\min,2})$. On the contrary, for a dryer but colder climate during the winter (Nancy and Madrid), the difference between both estimations is largely higher. The same trend can be found for Aix-en-Provence.

CONCLUSION

In this study, we have presented the hybrid solar road concept and its multi-physics modelization which couples thermal diffusion, hydraulic convection and radiative transfer. A numerical coupling based on the finite element method has been proposed and applied to compute the evolution of the temperature field in the structure under known environmental conditions. A command law has been presented to control the surface of the structure in temperature. The input fluid temperature is optimized with the adjoint state method by using the direct and adjoint models to prevent the surface from icing by keeping the temperature of the surface higher than a given threshold. The influence of the threshold was studied. Analysis of the results shows that under dry climates, the use of a dynamic threshold, based on the frozen point and also humidity, can highly reduce the need on heating. In prospect, other systems for the energy management of road structures will be led, particularly for electric solution or fluid flowing in tubes buried under the surface.

KEYWORDS
solar hybrid road, energy efficiency, computational methods, multi-physics heat transfer, finite element model, adjoint state method

REFERENCES
1. Asfour, S., Bernardin, F., Toussaint, E. and Piau, J.-M., Hydrothermal modeling of porous pavement for its surface de-freezing, Applied Thermal Engineering, Vol. 107, pp. 493-500, 2016
2. Bejan, A., Dincer, I., Lorente, S., Miguel, A. F. and Reis, A. H., Porous and Complex Flow Structures in Modern Technologies, Springer-Verlag New York, 1st edition, 2004
3. Buck, A. L., New equations for computing vapor pressure and enhancement factor, Journal of Applied Meteorology, Vol. 20, pp. 1527–1532, 1981
4. Chen, M., Wu, S., Wang, H. and Zhang, J., Study of ice and snow melting process on conductive asphalt solar collector, Solar Energy Materials and Solar Cells, Vol. 95, pp. 3241–3250, 2011
5. Duarte, F. and Ferreira, A., Energy harvesting on road pavements: state of the art. Proceedings of the institution of civil engineers, Vol. 169, pp. 79–90, 2016
6. `https://energyplus.net/weather`
7. Eugster, W. J., Road and Bridges Heating Using Geothermal Energy. Overview and Examples, Proceedings of European Geothermal Congress, Unterhaching, Germany, 2007
8. Hasebe, M. , Kamikawa, Y. and Meiarashi, S., Thermoelectric Generators using Solar Thermal Energy in Heated Road Pavement, Proceedings of the International Conference on Thermoelectrics, Vienna, Austria, pp. 697-700, 2006
9. Howell, J. R., Siegel, R. and Pinar, M. P., Thermal radiation heat transfer, 5th edition, CRC Press, Boca Raton, Florida, 2010
10. Incropera, F. P. and DeWitt, D. P., Fundamentals of heat and mass transfer, 3rd edition, Wiley, Hoboken, New Jersey, 1990
11. Johnson, C., Numerical solution of partial differential equations by the finite element method, 1st edition, Cambridge University Press, 1987
12. Le Touz, N., Dumoulin, J. and J.-M. Piau, tude numrique de la rsolution du couplage convection/radiation/diffusion dans une structure de chausse hybride, Proceedings of french thermal congress (SFT), 2017
13. Le Touz, N., Toullier, T. and Dumoulin, J., Infrared thermography applied to the study of heated and solar pavement: from numerical modeling to small scale laboratory experiment, Proceedings of SPIE-Thermosense: Thermal Infrared Applications XXXIX, Apr 2017, Anaheim, United States
14. Mallick, R. B., Chen, B.-L. and Bhowmick, S., Harvesting energy from asphalt pavements and reducing the heat island effect, International Journal of Sustainable Engineering, Vol. 2, No. 3, pp. 214-228, 2009
15. Nield, D. A. and Bejan, A., Convection in porous media, 4th edition, Springer, New York, 2013
16. Ping, T. H. and Lallemand, M., Transient radiative-conductive heat transfer in flat glasses submitted to temperature, flux and mixed boundary conditions, Int. J. Heat Mass Transfer, Vol. 32, No. 5, pp. 795–810, 1989
17. Taine, J., Enguehard, F. and Iacona, E., Transferts thermiques, introduction aux transferts d'nergie, 5th edition, Dunod, Paris, 2014